JACS
JOURNAL OF THE AMERICAN CHEMICAL SOCIETY
Article
pubs.acs.org/JACS

Contrasting Photophysical Properties of Star-Shaped vs Linear Perylene Diimide Complexes

Christopher M. Pochas,[‡] Kurt A. Kistler,[†] Hajime Yamagata,[†] Spiridoula Matsika,[†] and Frank C. Spano*[,†]

[†]Department of Chemistry, Temple University, Philadelphia, Pennsylvania 19122, United States
[‡]Department of Chemistry, Pennsylvania State University, Brandywine Campus, Media, Pennsylvania 19063, United States

Supporting Information

ABSTRACT: The absorption line shapes of a series of linear and star-shaped perylene diimide (PDI) complexes are evaluated theoretically and compared to experiment. The cyclic trimer and tetrahedral complexes are part of the symmetric series, characterized by a single interchromophoric coupling, J_0, between any two PDI chromophores. The measured spectra of all complexes show pronounced vibronic progressions based on the symmetric ring stretching mode at ~1400 cm^{-1}. The spectral line shapes are accurately reproduced using a Holstein Hamiltonian parametrized with electronic couplings calculated using time-dependent density functional transition charge densities. Although the "head-to-tail" linear complexes display classic J-aggregate behavior, the star-shaped complexes display a unique photophysical response, which is neither J- nor H-like. In the symmetric N-mers (N = 2−4), absorption and emission are polarized along $N - 1$ directions in contrast to linear complexes where absorption and emission remain polarized along the long molecular axis. In the symmetric complexes the red-shift of the 0−0 peak with increasing $|J_0|$, as well as the initial linear rise of the 0−0/1−0 oscillator strength ratio with increasing $|J_0|$, are independent of the number of PDI chromophores, N, and are markedly smaller than what is found in the linear series, where the shifts and ratios depend on N. Moreover, whereas the radiative decay rate, γ_r, scales with N and is therefore superradiant in linear complexes, γ_r scales with $N/(N - 1)$ in the symmetric complexes. Vibronic/vibrational pair states (two-particle states) are found to profoundly affect the absorption line shapes of both linear and symmetric complexes for sufficiently large coupling.

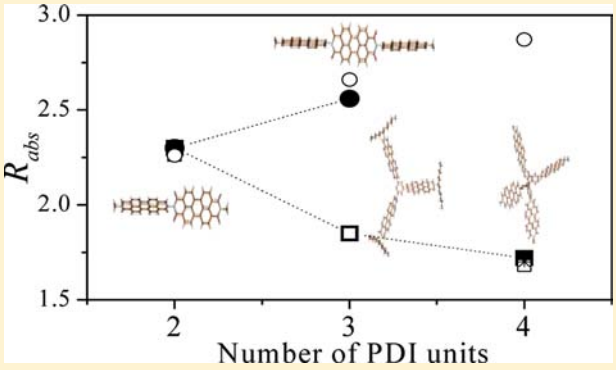

1. INTRODUCTION

Star-shaped complexes of π-conjugated chromophores are currently generating significant interest for use in optoelectronic devices,[1] which take advantage of isotropic absorption[2,3] and charge transport[4,5] without the sometimes disadvantageous effects of aggregation. Such molecules are also templates for higher-generation energy-funneling dendrimers, which are of significant interest theoretically[6−8] and practically as active materials for nonlinear optics, catalysis, drug delivery, and sensors.[8−10]

We present here a theoretical analysis of the excited states and absorption spectra of a series of linear and star-shaped covalently linked perylene diimide (PDI) complexes.[11−15] PDI-based chromophores have high quantum yields and well-resolved vibronic spectra and readily self-assemble into a variety of geometries leading to both J- and H-aggregates,[16−18] making them ideal chromophores for studying the impact of aggregation on photophysical properties. Covalently linked PDI complexes also display J- and H-aggregate behavior and serve as model systems with which to study charge transport,[11,19] excimer formation,[20,21] and energy migration.[22−25]

Previously, we conducted a theoretical investigation[26] of absorption and emission in a chiral PDI bichromophore,[27] using a Holstein Hamiltonian with a basis set consisting of single- and two-particle states. Electronic couplings were determined from time-dependent density functional (TDDFT) transition charge densities; that study quantitatively accounted for the Davydov splitting observed in the measured absorption spectrum[27] and showed that the spectral line shapes of the low- and high-energy Davydov components strongly resemble the line shapes expected for J- and H-aggregates, respectively. Here, we extend our investigation to include linear and higher-symmetry PDI complexes.[11−15]

The simplest molecule in the linear series is a head-to-tail dimer in which the two PDI's are covalently linked through the nitrogen head atoms. The addition of another PDI molecule using the same bonding motif results in the linear trimer.[11−13] The nonlinear complexes considered in this work include a cyclic trimer consisting of three PDI chromophores bound to a phenyl core[12,14] and a tetrahedral complex of phenyl-PDI chromophores linked to a central sp^3-hybridized carbon atom.[12,15] In such a symmetric series of star-shaped complexes the coupling between the constituent PDI chromophores is characterized by a single

Received: September 3, 2012
Published: February 12, 2013

   dx.doi.org/10.1021/ja3087449 | J. Am. Chem. Soc. 2013, 135, 3056−3066

value. For example, any of the four chromophores in the tetrahedral complex are coupled to any of the others with the same coupling constant. Note that the dimer is a member of both the linear and symmetric series.

In ref 12, Langhals observed that in chloroform solutions of the aforementioned linear and symmetric complexes, the peak molar absorptivity exceeds N times the peak absorptivity of monomeric PDI. Here, N is the number of PDI chromophores comprising the complex. Interestingly, the enhancement increases in going from the dimer to linear trimer but decreases in going from the dimer to the cyclic trimer. Such curious observations provided the stimulus for the present work. In what follows, we will show that the linear series exhibits canonical J-aggregate behavior, as expected for a head-to-tail arrangement of chromophores,[28] while the symmetric series shows entirely unique photophysical behavior, neither J- nor H-like. In the linear complexes, oscillator strength is concentrated in the transition to the lowest energy exciton which is nondegenerate. Absorption and emission are polarized entirely along the long molecular axis. Although the oscillator strength remains concentrated in the lowest energy exciton in the star-shaped trimers and tetramers, the degeneracy of the band-bottom exciton increases in going from the trimer (two-fold degenerate) to the tetramer (three-fold degenerate), leading to polarized absorption and emission along two and three molecular frame axes, respectively. Moreover, in the linear series the energy of the lowest energy exciton red-shifts with increasing N, consistent with what is expected for J-aggregates, whereas in the symmetric series the lowest energy exciton has no explicit N dependence. As we will find, fundamental differences in the exciton band structure endow the symmetric complexes with photophysical properties differing substantially from linear J-aggregates. With such differences at hand, we will evaluate the impact of molecular nonlinearity on the radiative decay rate and the efficiency of photon absorption, important considerations in solar cell design.

A secondary goal of the current analysis is to rigorously test the accuracy of our theoretical approach for evaluating the absorption spectral line shapes of molecular aggregates.[26] The approach begins with the calculation of the excitonic interactions between PM3-minimized chromophores using TDDFT determined transition-charge densities. The electronic couplings are subsequently inserted into a Holstein-like Hamiltonian for treating vibronic coupling involving the symmetric ring stretching mode. In what follows, our calculated spectra for the aforementioned PDI complexes will be compared directly to the measured spectra of Langhals et al.[12−15] We will also generalize a previously derived expression[29,30] for the ratio of 0−0 to 1−0 vibronic line strengths to include the symmetric PDI complexes. The formula is applicable whenever the exciton bandwidth is smaller than the nuclear relaxation energy and has been successfully applied to aggregates of conjugated polymers,[31] carotenoid assemblies,[32] and, most recently, to chiral PDI complexes.[26]

2. MODEL

In this section, we introduce the Hamiltonian for the geometry-optimized PDI complexes shown in Figure 1. Since the torsional angle between adjacent PDI chromophores is almost 90°, each PDI can be treated as an individual chromophore within a through-space coupled aggregate; excitations are therefore analogous to Frenkel excitons in molecular aggregates and crystals. In order to account for the linear electron-vibrational coupling involving the progression-forming ring stretching

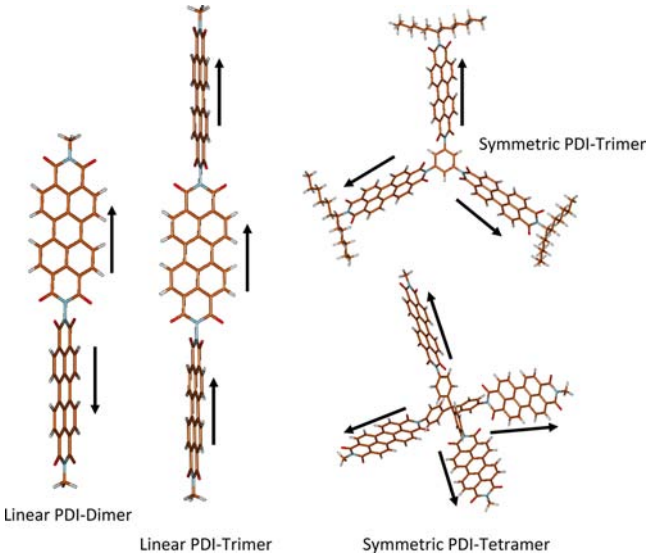

Figure 1. Geometry-optimized PDI complexes considered in this work. Also shown is our adapted phase convention, as indicted by the directions of the PDI transition dipole moments.

mode, we employ a site-based Holstein Hamiltonian, where the nuclear potentials for molecular vibrations in the ground (S_0) and excited (S_1) electronic states are shifted harmonic wells of identical curvature. In the vector subspace containing a single electronic excitation within an aggregate consisting of N PDI chromophores the Hamiltonian is

$$H = \hbar\omega_0 \sum_n b_n^\dagger b_n + \hbar\omega_0\lambda \sum_n (b_n^\dagger + b_n)|n\rangle\langle n| + \sum_{m,n} J_{mn}|m\rangle\langle n| + e_{0-0} + \hbar\omega_0\lambda^2 \quad (1)$$

The first term represents the vibrational energy, with the operators $b_n^\dagger$ and b_n, respectively creating and annihilating vibrational excitations in the nth PDI chromophore. The vibrational mode is taken to be the symmetric ring stretching mode with $\hbar\omega_0 = 1400\ \mathrm{cm}^{-1}$. The Huang−Rhys (HR) factor λ^2 is derived from the monomer absorption spectrum and was determined to be 0.60 (see below). The second term in eq 1 represents the linear vibronic coupling, while the third term represents excitonic coupling, with $|n\rangle$ indicating that chromophore n is in its electronic excited state (S_1) with all other PDI chromophores in their electronic ground states (S_0). J_{mn} is the excitonic coupling between chromophores n and m, and e_{0-0} represents the energy of the 0−0 transition of the single molecule in solution.

The basis set used to represent H in eq 1 consists of the so-called single- and two-particle states.[33,34] In a single-particle state, denoted as $|n, \tilde{\nu}\rangle$, the nth PDI chromophore is electronically excited with $\tilde{\nu}$ vibrational quanta in its shifted (S_1) potential well. The remaining $N - 1$ chromophores are in their vibrationless ground states. In a two-particle state, denoted $|n, \tilde{\nu}; n', \nu'\rangle$, chromophore n is electronically excited with $\tilde{\nu}$ excited-state vibrational quanta, while molecule n' is vibrationally excited with $\nu' > 0$ vibrational quanta in the S_0 potential. The remaining $N - 2$ chromophores are in their vibrationless ground states. Three- and higher particle states for complexes with three or more PDI's can also be included, but their impact is negligible.[33,35] The αth eigenstates of H in eq 1 can then be expanded as

dx.doi.org/10.1021/ja3087449 | J. Am. Chem. Soc. 2013, 135, 3056−3066

Table 1. J_{mm} for Pairs of Monomer PDIs for Each of the Systems in This Study: Dimer, Linear and Symmetric Trimers, and Symmetric Tetramer, Given in eV and cm^{-1} [a]

dimer	J/eV	J/cm^{-1}
J_{12}	0.05842	471.2

symmetric (cyclic) trimer	J/eV	J/cm^{-1}
J_{12}	0.02689	216.8
J_{13}	0.02654	214.1
J_{23}	0.02672	215.5

linear trimer	J/eV	J/cm^{-1}
J_{12}	−0.05842	−471.2
J_{13}	−0.00534	−43.0
J_{23}	−0.05846	−471.5

symmetric (tetrahedral) tetramer	J/eV	J/cm^{-1}	J/eV[b]	J/cm^{-1} [b]	PDI-PDI angles	angle/deg
J_{12}	0.01271	102.5	0.01479	119.3	∠12	103.771
J_{13}	0.01084	87.40	0.01315	106.0	∠13	112.301
J_{14}	0.01083	87.36	0.01317	106.2	∠14	113.298
J_{23}	0.01076	86.76	0.01304	105.2	∠23	112.700
J_{24}	0.01084	87.39	0.01312	105.8	∠24	111.987
J_{34}	0.01280	103.3	0.01486	119.9	∠34	103.157

[a]Unless otherwise stated, monomers are *N*,*N*-dimethyl PDIs. Also given for the symmetric tetramer are the angles between the long axes for each pair, in degrees. [b]Monomers are *N*-methyl-*N*-phenyl PDIs.

$$|\psi^{(\alpha)}> = \sum_{n,\tilde{\nu}} c^{(\alpha)}_{n,\tilde{\nu}} |n, \tilde{\nu}> + \sum_{n,\tilde{\nu}} \sum_{n'\nu'} c^{(\alpha)}_{n,\tilde{\nu};n,\nu'} |n, \tilde{\nu}; n', \nu'> \quad (2)$$

The expansion coefficients are readily determined numerically.

The method used here to calculate the excitonic coupling J_{mn} between PDI chromophores m and n has been described previously.[26] We briefly present the important points here. The structure for each of the PDI complexes in this report was optimized at the PM3 level (see Figure 1). Then, for each of the symmetric complexes, the N−C bond connecting the PDI to the central core is replaced with a methyl group. (For linear systems, the N−N bond is broken and terminated with a methyl group on each PDI.) If an alkyl chain is also attached to a PDI in the supersystem, it is also replaced by a methyl group. This creates independent *N*,*N*-dimethyl PDIs with their original PM3 geometries and orientations present in the super system. Ideally, coupling between these monomers would be calculated as the Coulombic interaction between their respective monomeric excited-state transition densities, but this would be a rather costly procedure. In order to mimic the spatial qualities of monomeric transition densities on each PDI chromophore, Mullikan population analysis (MPA) is applied to the monomeric transition density of the bright $\pi\pi^*$ excited state (S_1) for each PDI. This decomposes the monomeric transition density to point charges localized on each atom of the monomer, mimicking the extent of transition polarization each atom feels in the excitation and capturing much of the spatial character of the transition density. For this study, this was done by expanding the excited-state wave function in terms of its single-excitation Slater determinants and their corresponding CI coefficients from a TDDFT excited-state calculation using the hybrid functional B3LYP and the cc-pVDZ basis set.[36] This method has been used by others for calculating the coupling between carbon nanotubes within the TDDFT regime,[37] and it has been used with other single-reference excited-state methods.[37−40] The PDI transition dipole calculated using this method is on average about 8.4 D, close to the experimental value of 8.5 D. Further details can be found in ref 26.

Table 1 shows the calculated pairwise electronic couplings within each of the PDI complexes. In the case of the symmetric tetramer discussed in this report, two different sets of monomeric units were generated from the supersystem. One set generated was the *N*,*N*-dimethyl PDIs, described above, and the other included the phenyl attached to each PDI and the central carbon of the supersystem, generating four *N*-methyl-*N*-phenyl PDI monomers. For this set, the coordinates of the phenyl-PDIs were those from the PM3 structure of the supersystem, with the central C replaced by a reasonable phenyl C−H bond. This was done in order to study the influence of including the phenyl along with the PDI as a single monomeric chromophore and the effect this has on the coupling and resulting spectral predictions.

Table 1 shows that the PM3-minimized cyclic trimer and tetrahedral complexes are not fully symmetric, with slight differences in the intermolecular couplings within each complex. However, such differences are certainly smaller than kT at reasonable temperatures, allowing one to safely employ a mean coupling, J_0, to fully describe all interchromophore interactions within a symmetric trimer or tetramer. We verified in our spectral simulations that using the couplings in Table 1 produces spectra indistinguishable from those computed using the mean coupling, J_0, which preserves the symmetry of the complex.

In the symmetric series the wave function phase was chosen so that it is preserved under a rotation, i.e., $\hat{C}_{2,3}|n> = |m>$, where $\hat{C}_2$ and $\hat{C}_3$ are two- and three-fold rotational operations appropriate for the dimer ($\hat{C}_2$) and trimer and tetramer ($\hat{C}_3$). This leads to a similar relationship among the transition dipole moments $\hat{C}_{2,3}\vec{\mu}_m = \vec{\mu}_n$ such that all $\vec{\mu}_n$ point radially away from the molecular center, as indicated in Figure 1. Hence, in a dimer the positive coupling from Table 1 ($J_{12} > 0$) is consistent with the lowest energy exciton of the form, $2^{-1/2}(|1> - |2>)$, which is strongly allowed since the transition dipole moment is, $(\vec{\mu}_1 - \vec{\mu}_2)/\sqrt{2}$ ($= \sqrt{2}\vec{\mu}_1$). By contrast, the higher energy exciton, $2^{-1/2}(|1> + |2>)$ is optically forbidden. The PDI dimer is therefore an ideal J-aggregate. Note from Table 1 that a different but more conventional phase convention is employed for a linear trimer. Here, the phase of the three electronic wave functions $|n>$ ($n = 1-3$) is chosen such that the transition dipole moments are all parallel and unidirectional $\vec{\mu}_n = |\vec{\mu}_n|\hat{x}$, where $\hat{x}$ is a unit vector

dx.doi.org/10.1021/ja3087449 | J. Am. Chem. Soc. 2013, 135, 3056−3066

pointing along the long molecular axis (see Figure 1). With this convention the intermolecular couplings are now negative. However, the linear trimer, like the dimer, remains a J-aggregate since the (x-polarized) transition to the lowest energy exciton remains the most strongly allowed.

To begin, we consider the eigenstates and energies of just the excitonic part of the Hamiltonian, the third summation term in eq 1. Hence, all energies are relative to the monomer energy, e_{0-0}. For the symmetric series the energy levels are arranged as shown in Figure 2. The lower level is $(N-1)$-fold degenerate with

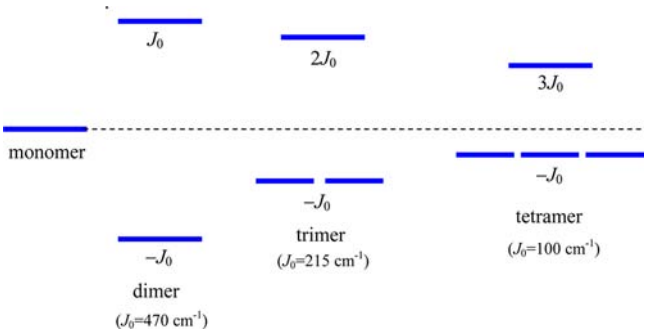

Figure 2. Exciton energy levels in the symmetric series of chromophores in the absence of vibronic coupling. For the dimer, trimer, and tetramer, the lower states are optically allowed from the ground state, while the upper state is optically forbidden. Generally, a symmetric N-mer has $N-1$ degenerate bright states at the band bottom. The unique coupling J_0 is evaluated numerically (see text) and is positive with our chosen phase convention. Note that the exciton bandwidth, NJ_0, decreases with increasing N.

energy $-J_0$, while the highest energy nondegenerate exciton has energy $(N-1)J_0$. Hence, if J_0 were constant throughout the series, the lowest energy would be independent of N, in stark contrast to the linear complexes (see below). In reality, J_0 itself diminishes with N, as shown by our transition-charge density calculations as described above (see Table 1), so that the level structure appears as shown in Figure 2. The exciton bandwidth, NJ_0, decreases with N because J_0 decreases faster than $1/N$.

The exciton wave functions corresponding to the states in Figure 2 are straightforward. The upper level exciton for all complexes in the symmetric series is nondegenerate, consisting of the totally symmetric combination of on site excitations, i.e., $\psi^N_{\text{upper}} = N^{-1/2}\sum_n |n>$. The transition dipole moment is exactly zero, as can be verified by taking a symmetric sum of the radially directed PDI transition dipole moments (see Figure 1).

For the dimer, the lowest energy exciton is the antisymmetric combination:

$$\psi^{N=2}_{\text{lower}} = \frac{1}{\sqrt{2}}\{|1> - |2>\}; \quad M_{2,x} = \sqrt{2}\mu \tag{3}$$

where we have indicated the nonzero component of the transition dipole moment, $M_{N,x}$. The lowest energy excitons for the symmetric trimer and tetramer are basis functions for the E and T irreducible representations of the D_{3h} and T point groups. Hence, for the cyclic trimer we have

$$\psi^{N=3}_{\text{lower},x} = \frac{1}{\sqrt{2}}\{|2> - |3>\}; \quad M_{3,x} = \sqrt{3/2}\mu$$
$$\psi^{N=3}_{\text{lower},y} = \frac{1}{\sqrt{6}}\{2|1> - |2> - |3>\}; \quad M_{3,y} = \sqrt{3/2}\mu \tag{4}$$

The transition dipole moments are evaluated by summing the individual PDI transition dipole moment vectors using the coefficients that appear in the wave function expansion. Finally, for the tetrahedral complex, the triply degenerate states with their transition dipole moments are

$$\psi^{N=4}_{\text{lower},x} = \frac{1}{2}\{|1> - |2> - |3> + |4>\}; \quad M_{4,x} = \sqrt{4/3}\mu$$
$$\psi^{N=4}_{\text{lower},y} = \frac{1}{2}\{|1> - |2> + |3> - |4>\}; \quad M_{4,y} = \sqrt{4/3}\mu$$
$$\psi^{N=4}_{\text{lower},z} = \frac{1}{2}\{|1> + |2> - |3> - |4>\}; \quad M_{4,z} = \sqrt{4/3}\mu \tag{5}$$

For the linear series the eigenspectra are quite different. Here, we consider nearest-neighbor coupling only, also designated as J_0, which is now negative ($J_0 < 0$), consistent with the usual phase convention for linear aggregates. The dimer's eigenspectrum was already discussed as a member of the symmetric series. For the linear (J-) aggregates with $N > 2$, the exciton energies (relative to the monomer e_{0-0}) are given by

$$\varepsilon^N_k = -2|J_0|\cos\left(\frac{k\pi}{N+1}\right), \quad N > 2 \tag{6}$$

where k indexes the eigenstates, $k = 1, \ldots, N$. The band structure is depicted in Figure 3. All eigenstates are nondegenerate. The

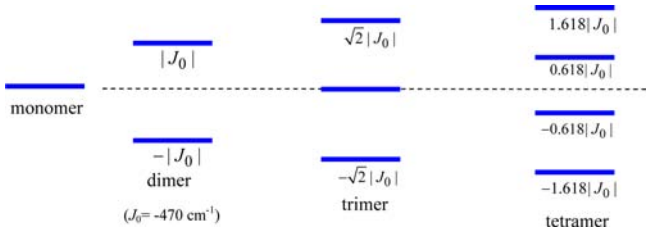

Figure 3. Exciton energy levels in the linear series of chromophores assuming nearest-neighbor-only coupling equal to J_0 and no vibronic coupling. Unlike the symmetric series, the value of J_0 remains constant throughout the series and the red shift of the lowest energy exciton increase with N. Consistent with our chosen phase convention for linear complexes, J_0 is negative (see text). In all cases the lowest energy exciton is the most strongly allowed from the ground state. Such complexes therefore behave as ideal J-aggregates.

wave functions, together with their transition dipole moments are

$$\psi^N_{\text{linear},k} = \sqrt{\frac{2}{N+1}}\sum_n \sin\frac{n\pi k}{N+1}|n> \tag{7}$$

$$M_{N,k,x} = \sqrt{\frac{2}{N+1}}\cot\left(\frac{\pi k}{2(N+1)}\right)\mu; \quad k = 1, 3$$
$$M_{N,k,x} = 0 \qquad k = 2, 4 \tag{8}$$

eq 8 shows that the line strength is mainly concentrated in the lowest energy exciton ($k = 1$), consistent with J-aggregation. This is readily seen in the limit $N \gg 1$, where

$$|M_{N,1,x}|^2 \approx 8\mu^2(N+1)/\pi^2 \tag{9}$$

The scaling of the squared transition dipole moment with N is a signature of superradiance.

dx.doi.org/10.1021/ja3087449 | J. Am. Chem. Soc. 2013, 135, 3056−3066

3. COMPARISON TO EXPERIMENT

Figure 4 shows the experimental absorption spectra of the symmetric series of PDI complexes dissolved in chloroform as

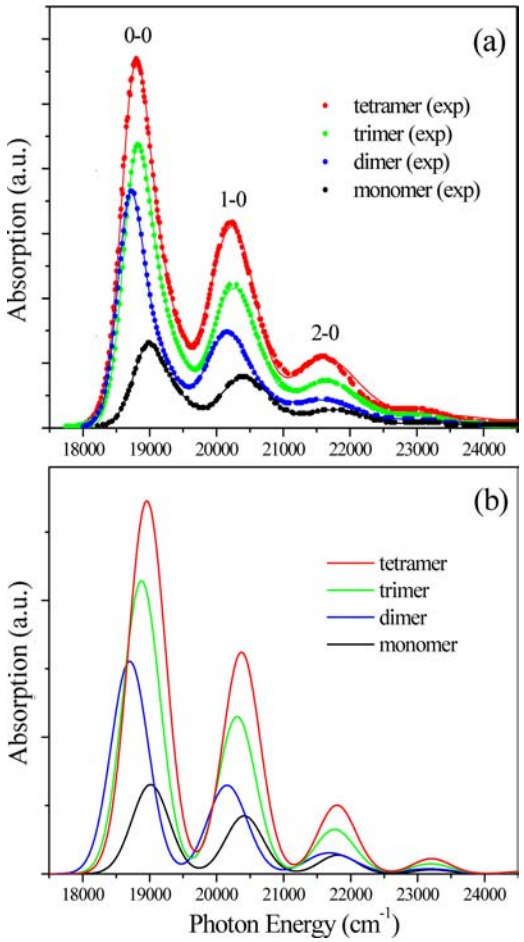

Figure 4. (a) Measured (dots) and fitted (lines) absorption spectra of the symmetric series of PDI complexes. (b) Calculated spectra using a Gaussian line shape in eq 11 with a full width (at the $1/e$ point) of 800 cm^{-1} (see text for details).

measured by Langhals et al.[12−15] In monomeric PDI, the vibronic peaks labeled as n−0 (n = 0, 1, 2, ...) correspond to transitions from the vibrationless electronic ground state (S_0) to the electronic excited state (S_1) with n vibrational quanta (i.e., $S_1(n) \leftarrow S_0(0)$). In higher complexes the origin of the peaks is more complex, but we retain the same notation.

The spectral intensity in Figure 4a is in units of molar absorptivity. Hence, if the interactions between PDI chromophores were absent, the spectrum for the N-mer would be approximately N times the monomer spectrum shown in black. As pointed out by Langhals[12] the spectra in Figure 4 are peculiar in that the peak 0−0 absorptivity for an N-mer, significantly exceeds N times that of the monomer. The enhancement is ∼1.39 in the dimer but diminishes with increasing N; for the symmetric trimer and tetramer the enhancement is respectively, 1.1 and 1.07. To check whether the enhanced peak height is due to increased oscillator strength in the 0−0 transition, one should determine how the 0−0 spectral area of the N-mer compares to the monomer. This is particularly important because the 0−0 line width (or, more generally, the line shape) is not uniform throughout the symmetric series. The line asymmetry is mainly due to the presence of additional low-frequency vibrations (<600 cm^{-1}) which have been identified in PDI monomers[41] and derivatives thereof.[42] To estimate the spectral areas, we fit the measured absorption spectrum for each of the chromophores using displaced Gaussians. The fitted spectra are drawn alongside the measured spectra in Figure 4a. (Further details of the fitting procedure are contained in the SI.) Using the fitted Gaussians, we computed the spectral area of the 0−0 line normalized to N times the corresponding monomer area

$$\mathrm{SA}_N \equiv \frac{\int A_N^{0-0}(\omega)\mathrm{d}\omega}{N\int A_{mon}^{0-0}(\omega)\mathrm{d}\omega} \tag{10}$$

The results are collected in Table 2, alongside the mean excitonic couplings from Table 1. The Table shows that the normalized 0−0 oscillator strength does indeed exceed N times the monomer in a manner which decreases with increasing N in the symmetric series.

Table 2. Experimental 0−0 Spectral Areas Normalized to N Times the Monomer 0−0 Spectral Area for the Symmetric Series[a]

	mean excitonic coupling, J_0 (cm^{-1})	normalized 0−0 spectral area, SA_N (exp)	normalized 0−0 oscillator strength (eq 15)
dimer	471	1.23	1.19
trimer	215	1.07	1.09
tetramer	92 (110)	1.05	1.04 (1.05)

[a]Also shown are the calculated 0−0 oscillator strengths (similarly normalized) using the mean couplings from column one. Values in parentheses correspond to the tetramer composed of PDI-phenyl chromophores (see Table 1).

The observed decrease in the normalized 0−0 oscillator strength with N correlates with the diminishing value of J_0 with increasing N as shown in Table 2. To better understand the nature of the effect, we calculated the absorption spectrum for an isotropic distribution of N-mers using

$$A_N(\omega) = \sum_{j=x,y,z}\sum_{\alpha} f_{G,\alpha}^{(j)} W_{\mathrm{LS}}(\omega - \omega_\alpha) \tag{11}$$

eq 11 contains the (normalized) j-polarized oscillator strength from the vibrationless electronic ground state $|G\rangle$ to the αth excited state $|\psi^{(\alpha)}\rangle$,

$$f_{G,\alpha}^{(j)} \equiv E_\alpha |\langle G|\hat{\mathrm{M}}_j|\psi^{(\alpha)}\rangle|^2 \tag{12}$$

where $E_\alpha = \hbar\omega_\alpha$ is the transition energy to state α and $\hat{\mathrm{M}}_j$ is the jth component of the transition dipole moment (tdm) operator, defined as

$$\hat{\mathrm{M}}_j \equiv \sum_{n=1,N} \{|g><n| + |n><g|\}\mu_{n,j} \tag{13}$$

In eq 13, $\mu_{n,j}$ is the jth component of the transition dipole moment of the nth chromophore of the complex (see Figure 1), referred to the molecular frame. In eq 13, $|g\rangle \equiv |g_1 g_2, ..., g_N\rangle$, is the pure electronic ground state of the complex. Hence, $|G>$ is the product of $|g\rangle$ and the vacuum vibrational state in which all N oscillators are in the lowest level of the S_0 nuclear potential. Finally, W_{LS} in eq 11 is a symmetric line shape function, taken here to be Gaussian.

The absorption spectrum as written in eq 11 correctly identifies the absorption line strength to a particular state α with

dx.doi.org/10.1021/ja3087449 | J. Am. Chem. Soc. 2013, 135, 3056−3066

the oscillator strength in eq 12. In our previous works we based our analysis on an absorption line strength depending solely on the square of the transition dipole moment, i.e., lacking the transition energy dependence in eq 12. Such an approximation is consistent with a Poissonian distribution of 0−*n* line strengths in the monomer spectrum, as is normally assumed.[43] However, as shown in detail in the SI, the error incurred in neglecting the energy dependence is entirely negligible—at most a few percent—basically because the vibrational energy ($\hbar\omega_0$) is far smaller than the 0−0 optical transition energy, e_{0-0}.

For an isotropic distribution of PDI monomers eq 11 reduces to

$$A_{\mathrm{mon}}(\omega) = \mu^2 \sum_{n=0,1,2,..} \{(\omega_{0-0}^{\mathrm{mon}} + n\omega_0)\lambda^{2n}e^{-\lambda^2}/n!\} \times W_{\mathrm{LS}}(\omega - \omega_{0-0} - n\omega_0) \quad (14)$$

a Poissonian distribution slightly weighted by the aforementioned transition energy dependence. From the measured monomer absorption spectrum we have, $e_{0-0}^{\mathrm{mon}} \equiv \hbar\omega_{0-0}^{mon}$ = 19 000 cm^{-1}, $\hbar\omega_0$ = 1400 cm^{-1}, and 1.54 for the ratio of the 0−0 to 1−0 peak areas. Inserting these values in eq 14 gives the best fit HR factor to be λ^2 = 0.60.

Based on eqs 11−14 the 0−0 oscillator strength of the symmetric *N*-mer, $I_{A,N}^{0-0}$, normalized to *N* times the 0−0 line strength of the monomer is given by

$$\frac{I_{A,N}^{0-0}}{NI_{A,\mathrm{mon}}^{0-0}} \equiv \frac{\sum_{\alpha=1,...,N-1}\sum_j f_{G,\alpha}^{(j)}}{Ne_{0-0}^{\mathrm{mon}}e^{-\lambda^2}\mu^2} \approx \frac{(N-1)|<G|\hat{M}_x|\psi^{(\alpha=1)}>|^2}{Ne^{-\lambda^2}\mu^2} \quad (15)$$

The first sum runs over the $N - 1$ degenerate excitons comprising the lowest energy level with polarizations assumed in the order *x*,*y*,*z*. Hence, the $N - 1$ prefactor accounts for the equivalent contributions from the additional polarization components (*y* and *z*) encountered when $N \geq 2$. Note that the theoretical enhancement reduces to unity in the limit of vanishing coupling between PDI chromophores. In this case,

$$|<G|\hat{M}_x|\psi^{(\alpha=1)}>|^2 = e^{-\lambda^2}|M_{N,x}|^2 = e^{-\lambda^2}\mu^2 N/(N-1) \quad (16)$$

where the $M_{N,x}$ are given in eqs 3−5. Substitution of eq 16 into eq 15 yields $I_{A,N}^{0-0}/NI_{A,\mathrm{mon}}^{0-0}$ = 1.

Table 2 also reports the ratios $I_{A,N}^{0-0}/NI_{A,\mathrm{mon}}^{0-0}$ calculated using eq 15 with the αth wave function computed by diagonalizing the Holstein Hamiltonian in eq 1 using the mean of the excitonic couplings from Table 2. The calculated values agree quite well with the measured values. As expected, the enhancement correlates with the strength of the exciton coupling, J_0.

Such an aggregation-induced enhancement of the 0−0 oscillator strength is also a property of linear J-aggregates, containing one molecule per unit cell.[30] Although the dimer is certainly a J-aggregate, the symmetric trimer and tetramer are not, since the lowest energy exciton is degenerate. Moreover, the 0−0 oscillator strength, although enhanced relative to the monomer, decreases in going from N = 2 to 4 since J_0 (see Table 2) itself decreases. This trend opposes what is found in linear J-aggregates, as we show below.

Because the oscillator sum rule requires that the enhanced 0−0 oscillator strength must come at the expense of the oscillator strength residing in the side-bands (1−0, 2−0, ...), a better indicator of *J*-like behavior is an increase in the ratio of the 0−0 to 1−0 oscillator strengths, $R_{abs} \equiv I_{A,N}^{0-0}/I_{A,N}^{1-0}$, with increased exciton coupling.[30] Using the fitted spectra in Figure 4a we evaluated R_{abs} from the 0−0 and 1−0 spectral areas. The results appear in Table 3 and Figure 5a. R_{abs} is largest in the dimer, subsequently diminishing in going to the (symmetric) trimer and then to the tetramer, as J_0 also diminishes.

Table 3. Experimental and Theoretical 0−0/1−0 Oscillator Strength Ratios, R_{abs}, for the Symmetric Series[a]

	monomer	dimer	trimer (S)	tetramer (S)
experimental R_{abs}	1.54	2.30	1.85	1.72
calculated R_{abs} (SP and TP)	1.54	2.26	1.85	1.68 (1.70)
calculated R_{abs} (SP only)	1.54	2.63	1.98	1.71 (1.75)
R_{abs} (perturbation theory)		2.70	1.98	1.71 (1.75)

[a]Calculated values of R_{abs} employ the mean couplings in Table 2. The most accurate calculation uses all single particle (SP) and two-particle (TP) basis functions. The perturbative calculations are discussed in Section 4 and are based on eq 23 using the couplings in Table 2.

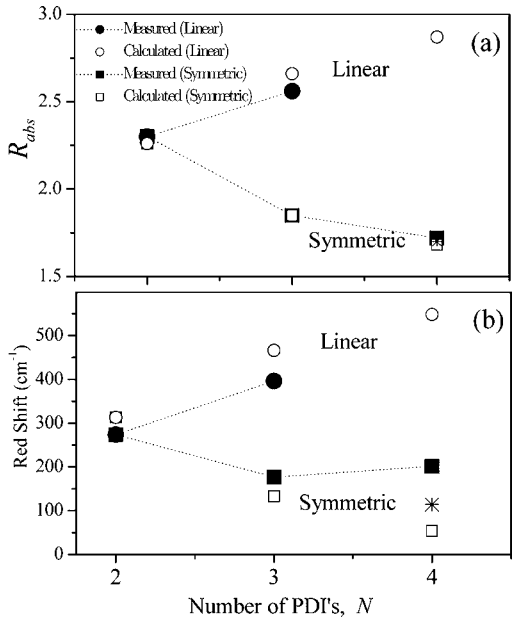

Figure 5. Measured and computed values of (a) R_{abs} and (b) the 0−0 spectral red-shift (relative to the monomer) in both the linear and symmetric series. Dotted lines connect the measured values. Computed shifts utilize the mean couplings in Table 2 for the symmetric series and the nearest-neighbor couplings in Table 4 for the linear series. All computations assume PDI complexes except the phenyl-PDI tetrahedral complex indicated by the asterisk (at N = 4).

The calculated values of R_{abs}, based on eigenstates and energies evaluated from the Hamiltonian in eq 1 with mean couplings taken from Table 2, are also shown in Table 3. Here, $I_{A,N}^{0-0}(I_{A,N}^{1-0})$ is obtained by summing $f_{G,\alpha}^{(j)}$ over all *j* and α, such that E_α lies within the 0−0 (1−0) bands. Table 3 and Figure 5a show that the agreement between the calculated and measured R_{abs} values is excellent.

We conclude our analysis of Langhal's symmetric series with Figure 5b, which shows the measured red-shift of the main 0−0 spectral peak relative to the monomer peak as a function of *N*. Traditionally, such spectral shifts have been used to extract the excitonic couplings. Comparison of the Langhals' data in Figure

dx.doi.org/10.1021/ja3087449 | J. Am. Chem. Soc. 2013, 135, 3056−3066

5a,b shows that the spectral shifts are strongly correlated to R_{abs}. Thus, within the symmetric series, the dimer undergoes the largest redshift with the largest R_{abs}. The reduction in the red-shift (and R_{abs}) in going from $N = 2$ and 3, coincides with the decrease in the TDDFT-calculated excitonic coupling J_0 (see Tables 1 and 2). The tetramer red-shift breaks the downward trend, being slightly greater than the trimer red-shift. This is likely due to the fact that the tetrahedral complexes of Langhals are composed of phenyl-PDI units (and not just PDI units as in the trimer) in which e_{0-0} is reduced mainly by nonresonant dispersion interactions and to a lesser extent by enhanced conjugation, although the latter is substantially compromised by the large dihedral angles between the phenyl and PDI groups (see Figure 1) . We note that the phenyl core within the trimer is expected to have a much smaller impact since there is only a single phenyl group per complex, and it is similarly disconnected from the PDI groups due to large dihedral angles.

Figure 5b also shows that our computed red shifts agree well with the measurements of Langhals. The calculated 60 cm^{-1} increase in the red-shift in the phenyl-PDI tetramer vs the PDI tetramer (the asterisk vs open square) is almost enough to account for the enhancement of the red-shift of the symmetric tetramer observed by Langhals. Figure 5a also shows that the ratio R_{abs} is practically independent of the extra phenyl group.

We now consider the linear series of PDI complexes which should behave as ideal J-aggregates. Figure 6a depicts the experimental spectra of Langhals et al.[12,13] along with our fitted spectra. Once again, as pointed out by Langhals, the 0−0 peak of the N-mer is enhanced relative to N times the 0−0 peak in the monomer. Figure 6b shows the calculated spectra based on the Hamiltonian in eq 1 and the spectrum in eq 11. The experimental enhancements of the 0−0 oscillator strength based on the fitted areas are tabulated in Table 4 alongside our calculated quantities.

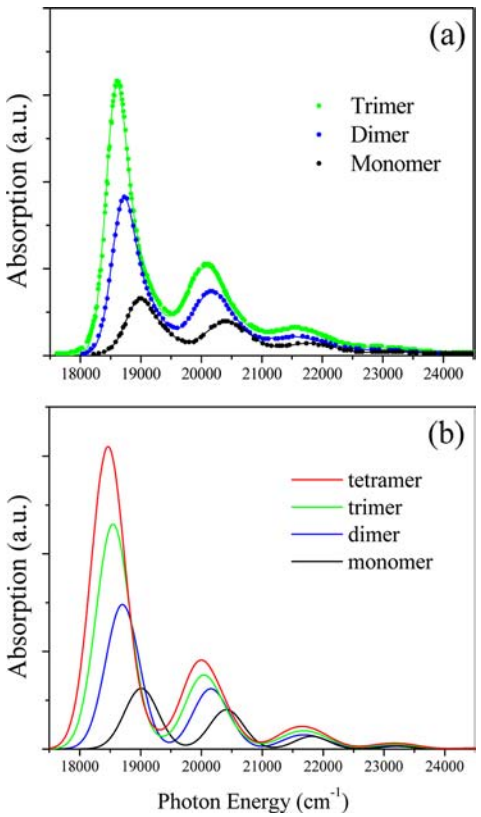

Figure 6. (a) Measured (dots) and fitted (lines) absorption spectra of the linear series of PDI complexes. (b) Calculated spectra using a Gaussian line shape in eq 11 with a full width (at $1/e$) of 800 cm^{-1} (see text for details).

Table 4. Experimental 0−0 Spectral Areas Normalized to N Times the Monomer 0−0 Spectral Area for the Linear Series[a]

	nearest-neighbor excitonic coupling (cm^{-1})	normalized 0−0 spectral area, SA_N (exp)	normalized 0−0 oscillator strength (calculated)
dimer	−471	1.23	1.19
trimer	−471	1.34	1.26
tetramer	−471	—	1.30

[a]Also shown are the calculated 0−0 oscillator strengths (similarly normalized).

In direct contrast to the symmetric series, the enhancement of the 0−0 peak in the linear trimer exceeds that in the dimer, as expected for J-aggregates. The trend is supported by our calculations up through the tetramer and correlates with a similar increase in the observed and calculated values of R_{abs}, as can be appreciated from Table 5 and Figure 5a. The behavior also correlates to an increase in the observed and calculated excitonic red-shift with N as shown in Figure 5b. The origin of the N-dependent shift can be traced back to the free-exciton regime of eq 6, where the $k = 1$ exciton's energy is given by, $-2|J_0|\cos(\pi/N + 1)$, see also Figure 3. The initial increase in the red shift with N directly contrasts what is found in the symmetric series (see Figure 5b) where the free-exciton energy is simply $-J_0$, with J_0 decreasing as N increases.

Table 5. Experimental and Theoretical 0−0/1−0 Integrated Line Strength Ratios for the Linear Series[a]

	monomer	dimer	trimer (L)	tetramer (L)
experimental R_{abs}	1.54	2.30	2.56	—
calculated R_{abs} (SP and TP)	1.54	2.26	2.66	2.87
calculated R_{abs} (SP only)	1.54	2.63	3.20	3.48
R_{abs} (perturbation theory)	—	2.65	3.26	3.60

[a]The most accurate calculation uses all SP and TP basis functions. The perturbative calculations are discussed in Section 4 and are based on eq 24.

In order to make a fairer comparison of the photophysical properties displayed by linear vs symmetric complexes we plot in Figure 7 the calculated values of R_{abs} vs $|J_0|$ for all of the complexes considered so far. The figure shows that in both series the ratio increases with $|J_0|$, as expected, with the linear complexes significantly exceeding their symmetric counterparts for a given $|J_0|$. Interestingly, the symmetric series is far less sensitive to J_0 and appears to converge with increasing J_0 . The ratio also converges in the linear series to the value of $N/(r_\omega\lambda^2)$ (but for larger values of $|J_0|$ than shown in Figure 7) as can be determined using Born−Oppenheimer approximation. (Here, r_ω is the ratio of the 1−0 and 0−0 peak absorption frequencies and is close to unity). For the symmetric series the converged value is approximately $N/[(N-1)\, r_\omega\, \lambda^2\,]$, obtained by replacing N in the linear series with $N/(N-1)$.

For a given value of $|J_0|$, opposite trends are observed with increasing N for the two series. Whereas R_{abs} increases with N in the linear series as expected for J-aggregates, it decreases with N in the symmetric series. Although the former dependence can be traced back to an increasing exciton bandwidth with N, the latter

dx.doi.org/10.1021/ja3087449 | J. Am. Chem. Soc. 2013, 135, 3056−3066

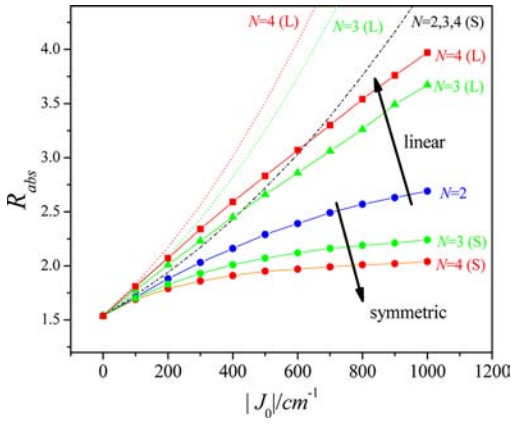

Figure 7. Calculated ratio of 0−0 and 1−0 oscillator strengths for the linear and symmetric series as a function of $|J_0|$ using $\lambda^2 = 0.60$. In the linear series the nearest-neighbor approximation was invoked with nearest-neighbor coupling equal to J_0 in Table 2. Dotted curves represent the single-particle approximation.

effect is quite unusual and arises entirely from two-particle states. This is readily appreciated from the curves in Figure 7 which are based on the single-particle approximation. In the symmetric series there is no N dependence at the single-particle level, ultimately due to the lack of any N dependence in the excitonic contribution to the energy of the optically allowed level. Hence, two-particle states have a more profound impact for complexes within the symmetric series.

4. WEAK COUPLING LIMIT: THE RATIO FORMULA

In this section we account for the observations in Section 3 by treating the excitonic Hamiltonian, H_{ex}, (third summation term in eq 1) as a perturbation, valid in the limit of weak excitonic coupling, $|J_0| \ll \lambda^2\hbar\omega_0$ The inequality is roughly satisfied by all of the PDI complexes considered so far. To zero-order in $|J_0|/\hbar\omega_0$, the eigenstates are divided into vibronic bands identified by the number of vibrational quanta, $\tilde{\nu} = 0, 1, 2, ...$, associated with the single-particle states with the greatest weighting. We begin our analysis with the symmetric series of chromophores, where the first-order corrected energies for the optically allowed levels are

$$E_{\tilde{\nu}} = e_{0-0} + \hbar\omega_0\tilde{\nu} - J_0\lambda^{2\tilde{\nu}}e^{-\lambda^2}/\tilde{\nu}!, \qquad \tilde{\nu} = 0, 1, 2, ... \tag{17}$$

Note that the levels in eq 17 are $(N-1)$-fold degenerate but otherwise do not depend on N. The associated zero-order wave functions are symmetry-adapted single-particle states resembling the excitonic wave functions in eqs 3−5. To first-order, like symmetry states in different bands couple together so that $\tilde{\nu}$ is no longer a good quantum number. Such interband coupling was discussed in detail in refs 29 and 44 for the case of linear aggregates. First-order coupling also connects the zero-order states with two-particle states, but the latter are dark and do not directly contribute to the absorption spectrum. (Their impact is, however, felt at higher orders.) The first-order corrected wave functions for the j-polarized optically allowed excitons are

$$|\psi_{\tilde{\nu},j}> \approx |\varphi_j, \tilde{\nu}> + \sum_{\tilde{\nu}'\neq\tilde{\nu}} \frac{<\varphi_j, \tilde{\nu}'|H_{ex}|\varphi_j, \tilde{\nu}>}{\hbar\omega_0(\tilde{\nu} - \tilde{\nu}')}|\varphi_j, \tilde{\nu}'>$$

$$\tilde{\nu} = 0, 1, 2, ... \tag{18}$$

where $j = x$ for the dimer, $j = x$ and y for the cyclic trimer, and $j = x$, y, and z for the tetrahedral complex, reflecting the increasing degeneracy of each vibronic level. The zero-order states $|\varphi_j, \tilde{\nu}>$ in eq 18 are delocalized single-particle states with expansion coefficients which come from the diagonalization of H_{ex} and hence are identical to those appearing in eqs 3−5. So, for example, in the tetrahedral complex the three degenerate zero-order excitons in the $\tilde{\nu}$ band are

$$|\varphi_x, \tilde{\nu}> = \frac{1}{2}\{|1, \tilde{\nu}> - |2, \tilde{\nu}> - |3, \tilde{\nu}> + |4, \tilde{\nu}>\} \tag{19a}$$

$$|\varphi_y, \tilde{\nu}> = \frac{1}{2}\{|1, \tilde{\nu}> - |2, \tilde{\nu}> + |3, \tilde{\nu}> - |4, \tilde{\nu}>\} \tag{19b}$$

$$|\varphi_z, \tilde{\nu}> = \frac{1}{2}\{|1, \tilde{\nu}> + |2, \tilde{\nu}> - |3, \tilde{\nu}> - |4, \tilde{\nu}>\} \tag{19c}$$

which are reminiscent of the sp^3-hybridized orbitals in tetrahedral carbon. (The fourth orbital corresponds to the higher energy optically forbidden exciton, see Figure 2.) Transitions to the excitons $|\psi_{\tilde{\nu}=0,j}>$ contribute to the 0−0 absorption band, while transitions to the excitons $|\psi_{\tilde{\nu}=1,j}>$ contribute to the 1−0 absorption band.

To first order in $(J_0/\hbar\omega_0)$ the 0−0/1−0 oscillator strength ratio, R_{abs}, is therefore

$$R_{abs} = \frac{E_{\tilde{\nu}=0}\sum_j |<G|\hat{M}_j|\psi_{\tilde{\nu}=0,j}>|^2}{E_{\tilde{\nu}=1}\sum_j |<G|\hat{M}_j|\psi_{\tilde{\nu}=1,j}>|^2} \tag{20}$$

After inserting the wave function in eq 18 into eq 20 one obtains, after some additional simplification, the final expression

$$R_{abs} = \frac{1}{\lambda^2 r_\omega}\left[\frac{(1 + G(0; \lambda^2)e^{-\lambda^2}J_0/\hbar\omega_0)}{(1 + G(1; \lambda^2)e^{-\lambda^2}J_0/\hbar\omega_0)}\right]^2, \qquad N = 2-4 \tag{21}$$

where $J_0 > 0$. The vibronic factors appearing in eq 21 are given by[29]

$$G(\tilde{\nu}; \lambda^2) \equiv \sum_{\substack{\tilde{\nu}'=0,1,2... \\ \tilde{\nu}'(\neq\tilde{\nu})}} \frac{\lambda^{2\tilde{\nu}'}}{\tilde{\nu}'!(\tilde{\nu}' - \tilde{\nu})} \tag{22}$$

The factor r_ω appearing in eq 21 arises from the transition frequency dependence of the oscillator strength. It is essentially the ratio of the 1−0 and 0−0 peak absorption frequencies in the monomer, which, for the present case is close to unity, $r_\omega \approx 1.07$. Our previous ratio expression[29] lacks r_ω, and it might be expected the deviation from the more accurate ratio in eq 21 is about 7% in the present case. The error is in fact much smaller, because neglecting the frequency dependence of the oscillator strength forces a slightly larger HR factor, equal to $\lambda^2 r_\omega$, to reproduce R_{abs} in the monomer spectrum. More details can be found in the SI.

Eq 21 (without r_ω) reduces to our previous expression for linear aggregates with periodic boundary conditions if the excitonic energy of the optically allowed (free-) exciton, $-J_0$ in eq 21, is replaced by the excitonic energy of the $k = 0$ exciton in the linear complex, $\tilde{J}_{k=0} \equiv \sum_n J_{mn}$, where the sum includes all neighbors (the two nearest and beyond) in the linear chain.[30] Hence, in all cases the ratio strictly depends on the excitonic shift

dx.doi.org/10.1021/ja3087449 | J. Am. Chem. Soc. 2013, 135, 3056−3066

of the optically allowed exciton, the magnitude of which is equal to half the exciton bandwidth only under the nearest-neighbor-only approximation.

When the HR factor for monomeric PDI, λ^2=0.60, is inserted into eq 22 we obtain, $G(0;0.60) = 0.703$ and $G(1;0.60) = -0.800$. Inserting these quantities into eq 21 gives the final first-order expression for the PDI symmetric series:

$$R_{abs} = 1.54\left[\frac{(1 + 0.386J_0/\hbar\omega_0)}{(1 - 0.439J_0/\hbar\omega_0)}\right]^2, \quad N = 2-4 \tag{23}$$

Since $J_0 > 0$, R_{abs} increases with J_0, as is also the case of J-aggregates. Unlike J-aggregates, however, there is no N dependence. The accuracy of eq 23 can be gauged from Tables 3 and 5.

Figure 8 shows R_{abs} plotted for small values of $|J_0|$ for the symmetric (and linear) series. The figure shows the ratios

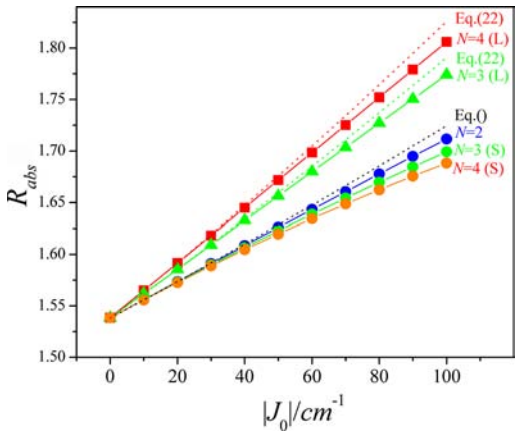

Figure 8. Calculated ratio of 0−0 and 1−0 oscillator strengths for the linear and symmetric series as a function of J_0. In the linear series the nearest-neighbor approximation was invoked with nearest-neighbor coupling equal to J_0. Dotted curves represent the perturbative expressions (see text).

calculated fully numerically (including single- and two-particle basis functions) and by using the first-order expression in eq 23. The latter works quite well when $J_0 < 100$ cm^{-1}. In the symmetric series there is practically no N dependence over the first 50 cm^{-1}, as predicted by eq 23. This can be ultimately traced back to the independence of the lowest exciton energy on N; see eq 17. For higher coupling strengths the ratio acquires an N dependence, being larger for the dimer and smallest for the tetramer. The N dependence arises entirely from the increased contribution of two-particle states, as discussed in the previous section.

The perturbation theory result for the linear series is more complex than its symmetric series counterpart, since oscillator strength is divided among the $k = 1$ and 3 excitons for both the $N = 3$ and 4 complexes (see eq 8). The division is purely a result of open boundary conditions. Assuming only nearest-neighbor coupling equal to $-|J_0|$ we obtain

$$R_{abs}(N) = \frac{1}{\lambda^2 r_\omega}\left[\frac{\sum_{k=1,3} M^2_{N,k,x}(1 - G(0;\lambda^2)e^{-\lambda^2}\varepsilon_k^N/\hbar\omega_0)^2}{\sum_{k=1,3} M^2_{N,k,x}(1 - G(1;\lambda^2)e^{-\lambda^2}\varepsilon_k^N/\hbar\omega_0)^2}\right] \tag{24}$$

which now depends on N through the transition dipole moments and energies from eq's 8 and 6, respectively. Since the energies are negative, eq 24 predicts J-aggregate behavior, with R_{abs} increasing with $|J_0|$. The ratios calculated using eq 24 are also plotted in Figure 8.

The initial linear rise of R_{abs} with $|J_0|$ is identical for all of the molecules in the symmetric series and is significantly smaller than the initial rise displayed by the linear trimer and tetramer. Using eqs 21 and 24 the initial slopes of all curves in Figure 8 are given by

$$\frac{dR_{abs}}{d|J_0|} = 2b\{G(0,\lambda^2) - G(1,\lambda^2)\}e^{-\lambda^2}/\hbar\omega_0\lambda^2 r_\omega \tag{25}$$

where the prefactor b is unity for all molecules in the symmetric series. For the linear trimer and tetramer b is, respectively, 1.33 and 1.55 and reflects the increase in the magnitude of the excitonic shift of the band bottom exciton with N. In the limit of large N, b approaches the value of two in the linear series since in this limit the lowest energy exciton approaches $-2|J_0|$ (see eq 6), twice as large (in magnitude) as what is found in the symmetric complexes.

5. DISCUSSION AND CONCLUSION

The photophysical properties of symmetric star-shaped chromophores are markedly different from their linear counterparts. The latter behave as J-aggregates, with oscillator strength concentrated in the transition to the lowest energy, non-degenerate exciton. The oscillator strength is linear with the number of chromophores N, which leads to superradiance at sufficiently low temperatures. By contrast, in the symmetric series of chromophores ($N = 2-4$) the lowest energy exciton level is $(N - 1)$-fold degenerate, supporting absorption and emission polarized in $N - 1$ orthogonal directions. The oscillator strength scales as $N/(N - 1)$ in each of the allowed directions. Hence, the overall emission decay rate also scales as $N/(N - 1)$, significantly weaker than the N-enhancement found in the linear complexes. The two sets of behaviors converge when $N = 2$, as expected since the dimer is a member of both series. In all linear and symmetric complexes the 0−0 peak in the absorption spectrum red shifts with increasing $|J_0|$ and the 0−0/1−0 oscillator strength ratio, R_{abs}, initially increases linearly with $|J_0|$. However, in the symmetric complexes these increases are independent of the number of PDI chromophores, N, and the spectral shifts and ratios are markedly smaller than in their linear counterparts (see Figure 8). In the linear complexes the excitonic red-shift and R_{abs} depend on both J_0 and N.

The opposing N-dependent behaviors observed in the absorption spectra of the symmetric vs linear series of PDI chromophores measured by Langhals et al.[12−15] and summarized in Figure 5 can be understood from the following trends: (1) In the symmetric series the coupling, J_0 (with $J_0 > 0$) diminishes with N, as confirmed through TDDFT calculations, but the excitonic (red) shift contains no topological N dependence. This is easily appreciated in the free-exciton regime where the excitonic shift for all optically allowed excitons is given simply by $-J_0$ for $N = 2-4$ (see Figure 2); (2) by contrast, in the linear series, the nearest-neighbor coupling J_0 remains constant, but the excitonic shift contains a topological N dependence of the form contained in eq 6, see also Figure 3. Hence, the observed increase in the 0−0 transition frequency along with the diminished value of R_{abs} in going from the dimer to the *cyclic* trimer are due to a decrease in J_0 (see Figure 4a), whereas the opposite behavior

dx.doi.org/10.1021/ja3087449 | J. Am. Chem. Soc. 2013, 135, 3056−3066

observed in going from dimer to *linear* trimer is due to the influence of the topological factor, for example, in the free-exciton limit the energy of the $k = 1$ exciton changes from $e_{0-0} - |J_0|$ for $N = 2$ to $(e_{0-0} - \sqrt{2}|J_0|)$ for $N = 3$. (The red-shift of the 0–0 peak in Langhals' tetrahedral complex breaks the symmetric trend and is actually slightly red-shifted compared with the cyclic trimer. This arises because the complex is composed of PDI-phenyl chromophores, with the extra phenyl unit per chromophore leading to an additional red-shift, see Figure 5.)

A very recent single-molecule study of linear and cyclic PDI trimers[25] showed that in roughly 20% of the cyclic trimers studied, the emission spectra of the trimer and dimer, where the latter is formed by photobleaching a single PDI unit within the trimer, are spectrally aligned (no relative shift), while a substantial blue shift occurs between the dimer and the monomer formed by photobleaching two PDI units. Such behavior is consistent with the energy level structure of Figure 2 but with a constant value of J_0, since the dimer formed upon photobleaching the trimer is necessarily bent with the same inter-PDI coupling as exists in the trimer. In ref 25 there are also molecules in which a blue-shift is observed in the emission spectrum upon photobleaching the trimer to create the dimer. Such cases may involve distorted trimers, where an angle between two of the three PDI units is contracted below 120° due to disorder-induced environmental factors. Almost half of the linear trimers in ref 25 showed a blue shift after both photobleaching events, as is consistent with the energy scheme in Figure 3.

We have shown previously that in linear J-aggregates with periodic boundary conditions the ratio of 0–0 and 0–1 line strengths in the PL spectrum, $I_{PL}^{0-0}/I_{PL}^{0-1}$, is equal to N/λ^2 whenever the exciton coherence covers all N chromophores, which is favored by low temperature and minimal disorder.[45] The N scaling was confirmed in the emission spectra of the photobleached linear trimers in ref 25. We have shown numerically that the PL ratio in symmetric complexes is, to an excellent approximation, given by $N/[(N-1)\lambda^2]$, thereby leading to a factor of 2 reduction in the PL ratio of the cyclic trimer compared to the linear trimer. (In fact, the reduction is slightly less than two due to end effects present in the linear trimer.) In ref 25 the maximum observed PL ratio in the linear trimers is ~4, compared to 2.7 in the cyclic trimers, in rough agreement with our predictions. A better agreement should be achieved by averaging over a Boltzmann distribution of emitting excitons as is necessary for $T > 0$ K.

Our analysis of spectra of Langhals et al.[12−15] also confirms an important correlation between the exciton red-shift of the 0–0 peak and the 0–0/1–0 ratio of oscillator strengths, R_{abs}, best demonstrated in Figure 5. Both quantities can be used to deduce the excitonic coupling, but R_{abs} is more reliable since there are additional sources to spectral shifts (i.e., the gas-to-crystal shift) which complicate the spectral-shift analysis. The spectral shift/R_{abs} correlation is evident in the perturbative expressions for R_{abs} in eqs 21 and 24, where R_{abs} is an increasing function of the magnitude of the (free-) exciton shift, for example R_{abs} increases with J_0 in eq 21. For the symmetric complexes, where the red-shift, $-J_0$, is independent of N, this suggests that in the perturbative regime, the absorption spectral line shapes for all symmetric complexes are identical, given a constant value of J_0 (see Figure 8). This is in fact the case, as we have confirmed numerically. This behavior is in stark contrast to the case of linear complexes where a strong N dependence arises from $\varepsilon_{k=1}^{N}$. Increasing J_0 in either series leads to a breakdown of the ratio formula as the two-particle contributions become important. In the symmetric complexes (with J_0 held constant), two-particle states cause a differentiation of the absorption line shapes for different N; the 0–0/1–0 ratios diminish with increasing N, exactly opposite to what is found in linear complexes. This behavior is shown in Figure 7, further demonstrating that symmetric complexes are unusual photophysical entities which are quite different from the conventional J- (or H-) aggregates.

It is interesting to compare linear vs star-shaped chromophores as light harvesters in solar cell applications. For an isotropic distribution of a given concentration of either chromophore type which is superior? By the oscillator sum rule, the integrated molar absorptivity is the same for a given N, but the distribution of oscillator strength is very different in the two chromophore types. In the linear series only the x-component (long-molecular axis) is optically allowed, whereas in symmetric molecules, oscillator strength is distributed over $N - 1$ orthogonal polarizations. Hence, in an isotropic distribution of either chromophore, the absorptivity along any particular direction is the same. The situation is entirely different in the crystal phase. Due to their geometry, linear chromophores are more prone to crystallization making absorption a strong function of the angle between the electric field vector and the crystal axes. Star-shaped molecules often resist crystallization, forming largely amorphous films. Thus, such films would not require solar tracking, in contrast to crystalline films, a point originally emphasized by Langhals.[12] Moreover, the significantly reduced radiative decay rates in the nonlinear complexes inhibits radiative loss. Hence, as solar harvesters, star-shaped molecules have significant advantages over their linear counterparts.

The accurate reproduction of the measured absorption spectral line shapes for the linear and symmetric complexes studied herein is strong validation for our computational method for evaluating interchromophore interactions as well as the application of the Holstein Hamiltonian for including the effects of the vibronic coupling. We have achieved a level of accuracy (with no adjustable parameters) of several percent in systems in which interchromophore interactions are dominated by through-space Coulombic interactions. For the PDI complexes studied here, the minimal cofacial overlap inhibits the involvement of charge transfer states[46] which are not accounted for in our analysis. Although in sandwich PDI complexes,[17,21,41,47] our analysis remains qualitatively correct, for example, it predicts a 0–0/1–0 ratio smaller than what is found in the monomer absorption spectrum, as expected for H-aggregates; it generally cannot account for the excimer-like PL line shapes[21,48] which contrast the well-structured vibronic PL line shapes found in the complexes studied here.[15,25] In future studies we will consider how vibronic coupling impacts energy and charge migration in PDI complexes.[11,19,22−24] It may also prove rewarding to investigate vibronic coupling in more elaborate architectures, such as dendrimers.

■ ASSOCIATED CONTENT

Ⓢ Supporting Information

Additional information about our spectral fitting procedure as well as a more detailed analysis of the impact of replacing the oscillator strength with the square of the transition dipole moment on the absorption spectral line shape. Atomic coordinates and ground state energies of the PM3 geometry-optimized structures for all of the PDI complexes studied herein. This material is available free of charge via the Internet at http://pubs.acs.org.

AUTHOR INFORMATION

Corresponding Author

spano@temple.edu

Notes

The authors declare no competing financial interest.

ACKNOWLEDGMENTS

F.C.S is supported by the National Science Foundation, grant no. DMR-1203811. S.M. is supported by the National Science Foundation, grant no. CHE-1213614.

REFERENCES

(1) Kanibolotsky, A. L.; Perepichka, I. F.; Skabara, P. J. *Chem. Soc. Rev.* **2010**, *39*, 2695.
(2) Oldham, W. J.; Lachicotte, R. J.; Bazan, G. C. *J. Am. Chem. Soc.* **1998**, *120*, 2987.
(3) Robinson, M. R.; Wang, S.; Bazan, G. C.; Cao, Y. *Adv. Mater.* **2000**, *12*, 1701.
(4) Roncali, J.; Leriche, P.; Cravino, A. *Adv. Mater.* **2007**, *19*, 2045.
(5) Mangold, H. S.; Richter, T. V.; Link, S.; Wurfel, U.; Ludwigs, S. *J. Phys. Chem. B* **2011**, *116*, 154.
(6) Tretiak, S.; Chernyak, V.; Mukamel, S. *J. Phys. Chem. B* **1998**, *102*, 3310.
(7) Minami, T.; Tretiak, S.; Chernyak, V.; Mukamel, S. *J. Lumin.* **2000**, *87*−*9*, 115.
(8) Badaeva, E.; Harpham, M. R.; Guda, R.; Suzer, O.; Ma, C. Q.; Bauerle, P.; Goodson, T.; Tretiak, S. *J. Phys. Chem. B* **2010**, *114*, 15808.
(9) Lee, C. C.; MacKay, J. A.; Frechet, J. M. J.; Szoka, F. C. *Nat. Biotechnol.* **2005**, *23*, 1517.
(10) Crooks, R. M.; Zhao, M. Q.; Sun, L.; Chechik, V.; Yeung, L. K. *Acc. Chem. Res.* **2001**, *34*, 181.
(11) Wilson, T. M.; Tauber, M. J.; Wasielewski, M. R. *J. Am. Chem. Soc.* **2009**, *131*, 8952.
(12) Langhals, H. *Helv. Chim. Acta* **2005**, *88*, 1309.
(13) Langhals, H.; Jona, W. *Angew. Chem., Int. Ed.* **1998**, *37*, 952.
(14) Langhals, H.; Gold, J. *J. Prakt. Chem./Chem.-Ztg.* **1996**, *338*, 654.
(15) Langhals, H.; Wagner, C.; Ismael, R. *New J. Chem.* **2001**, *25*, 1047.
(16) Kaiser, T. E.; Stepanenko, V.; Wurthner, F. *J. Am. Chem. Soc.* **2009**, *131*, 6719−6732.
(17) Ghosh, S.; Li, X.-Q.; Stepanenko, V.; Wurthner, F. *Chem.—Eur. J.* **2008**, *14*, 11343−11357.
(18) Shaller, A. D.; Wang, W.; Gan, H. Y.; Li, A. D. Q. *Ang. Chem. Int. Ed.* **2008**, *47*, 7705.
(19) Rybtchinski, B.; Sinks, L. E.; Wasielewski, M. R. *J. Phys. Chem A* **2004**, *108*, 7497.
(20) Veldman, D.; Chopin, S. M. A.; Meskers, S. C. J.; Groeneveld, M. M.; Williams, R. M.; Janssen, R. A. J. *J. Phys. Chem A* **2008**, *112*, 5846.
(21) Giaimo, J. M.; Lockard, J. V.; Sinks, L. E.; Scott, A. M.; Wilson, T. M.; Wasielewski, M. R. *J. Phys. Chem. A* **2008**, *112*, 2322.
(22) Schlosser, F.; Sung, J.; Kim, P.; Kim, D.; Wurthner, F. *Chem. Sci.* **2012**, *3*, 2778.
(23) Montgomery, N. A.; Hedley, G. J.; Ruseckas, A.; Denis, J.-C.; Schumacher, S.; Kanibolotsky, A. L.; Skabara, P. J.; Galbraith, I.; Turnbull, G. A.; Samuel, I. D. W. *Phys. Chem. Chem. Phys.* **2012**, *14*, 9176.
(24) Metivier, R.; Nolde, F.; Mullen, K.; Basche, T. *Phys. Rev. Lett.* **2007**, *98*, 047802.
(25) Yoo, H.; Furumaki, S.; Yang, J.; Lee, J.-E.; Chung, H.; Oba, T.; Kobayashi, H.; Rybtchinski, B.; Wilson, T. M.; Wasielewski, M. R.; Vacha, M.; Kim, D. *J. Phys. Chem. B* **2012**, *116*, 12878.
(26) Kistler, K. A.; Pochas, C. M.; Yamagata, H.; Matsika, S.; Spano, F. C. *J. Phys. Chem. B* **2011**, *116*, 77.
(27) Langhals, H.; Hofer, A.; Bernhard, S.; Siegel, J. S.; Mayer, P. *J. Org. Chem.* **2011**, *76*, 990.
(28) Kasha, M. *Radiat. Res.* **1963**, *20*, 55.
(29) Spano, F. C. *Chem. Phys.* **2006**, *325*, 22.
(30) Spano, F. C. *Acc. Chem. Res.* **2010**, *43*, 429.
(31) Clark, J.; Silva, C.; Friend, R. H.; Spano, F. C. *Phys. Rev. Lett.* **2007**, *98*, 206406.
(32) Spano, F. C. *J. Am. Chem. Soc.* **2009**, *131*, 4267.
(33) Spano, F. C. *J. Chem. Phys.* **2002**, *116*, 5877.
(34) Philpott, M. R. *J. Chem. Phys.* **1971**, *55*, 2039.
(35) Stradomska, A.; Petelenz, P. *J. Chem. Phys.* **2009**, *131*, 044507.
(36) Dunning, T. H. *J. Chem. Phys.* **1989**, *90*, 1007.
(37) Wong, C. Y.; Curutchet, C.; Tretiak, S.; Scholes, G. D. *J. Chem. Phys.* **2009**, *130*, 081104.
(38) Chang, J. C. *J. Chem. Phys.* **1977**, *67*, 3901.
(39) Patwardhan, S.; Sengupta, S.; Wurthner, F.; Siebbeles, L. D. A.; Grozema, F. *J. Phys. Chem. C* **2010**, *114*, 20834.
(40) Li, H.; Malinin, S. V.; Tretiak, S.; Chernyak, V. Y. *J. Chem. Phys.* **2010**, *132*, 124103.
(41) Guthmuller, J.; Zutterman, F.; Champagne, B. *J. Chem. Phys.* **2009**, *131*, 154302.
(42) Diehl, F. P.; Roos, C.; Jankowiak, H. C.; Berger, R.; Kohn, A.; Diezemann, G.; Basche, T. *J. Phys. Chem B* **2010**, *114*, 1638.
(43) Pope, M.; Swenberg, C. E. *Electronic processes in organic crystals and polymers*, 2nd ed.; Oxford University Press: New York, 1999; Vol. *56*.
(44) Spano, F. C. *J. Chem. Phys.* **2005**, *122*, 234701.
(45) Spano, F. C.; Yamagata, H. *J. Phys. Chem. B* **2011**, *115*, 5133−5143.
(46) Gao, F.; Zhao, Y.; Liang, W. *J. Phys. Chem. B* **2011**, *115*, 2699.
(47) Zheng, Y.; Long, H.; Schatz, G. C.; Lewis, F. D. *Chem. Commun.* **2005**, 4795−4797.
(48) Fink, R. F.; Seibt, J.; Engel, V.; Renz, M.; Kaupp, M.; Lochbrunner, S.; Zhao, H. M.; Pfister, J.; Wurthner, F.; Engels, B. *J. Am. Chem. Soc.* **2008**, *130*, 12858.